Aberrant Neuregulin 1/ErbB Signaling in Charcot-Marie-Tooth Type 4D Disease

Li-Ting Jiang,[a] Yu-Hui Chen,[a] Jie-Hong Huang,[a] Wei-Fang Tong,[a] Ling-Jing Jin,[b,c] Li-Xi Li[a]

[a]Department of Neurology, Tongji Hospital, School of Medicine, Tongji University, Shanghai, China
[b]Department of Neurorehabilitation, Shanghai Yangzhi Rehabilitation Hospital, School of Medicine, Tongji University, Shanghai, China
[c]Shanghai Clinical Research Center for Aging and Medicine, Shanghai, China

Li-Ting Jiang and Yu-Hui Chen contributed equally to this article. Author order was determined based on seniority.

ABSTRACT Charcot-Marie-Tooth type 4D (CMT4D) is an autosomal recessive demyelinating form of CMT characterized by progressive motor and sensory neuropathy. N-myc downstream regulated gene 1 (*NDRG1*) is the causative gene for CMT4D. Although more CMT4D cases have been reported, the comprehensive molecular mechanism underlying CMT4D remains elusive. Here, we generated a novel knockout mouse model in which the fourth and fifth exons of the *Ndrg1* gene were removed. *Ndrg1*-deficient mice develop early progressive demyelinating neuropathy and limb muscle weakness. The expression pattern of myelination-related transcriptional factors, including SOX10, OCT6, and EGR2, was abnormal in *Ndrg1*-deficient mice. We further investigated the activation of the ErbB2/3 receptor tyrosine kinases in *Ndrg1*-deficient sciatic nerves, as these proteins play essential roles in Schwann cell myelination. In the absence of NDRG1, although the total ErbB2/3 receptors expressed by Schwann cells were significantly increased, levels of the phosphorylated forms of ErbB2/3 and their downstream signaling cascades were decreased. This change was not associated with the level of the neuregulin 1 ligand, which was increased in *Ndrg1*-deficient mice. In addition, the integrin $\beta4$ receptor, which interacts with ErbB2/3 and positively regulates neuregulin 1/ErbB signaling, was significantly reduced in the *Ndrg1*-deficient nerve. In conclusion, our data suggest that the demyelinating phenotype of CMT4D disease is at least in part a consequence of molecular defects in neuregulin 1/ErbB signaling.

KEYWORDS Charcot-Marie-Tooth, NDRG1, demyelination, neuregulin 1, ErbB

Charcot-Marie-Tooth disease type 4D (CMT4D) is an autosomal recessive demyelinating neuropathy caused by mutations in *NDRG1* (1). Individuals affected by CMT4D present early-onset and severe motor and sensory neuropathy. The typical clinical manifestations include muscle weakness in the distal lower limbs in the first decade and then the upper limbs, skeletal and foot deformities, and sensorineural loss with deafness. Sural nerve biopsy studies of patients showed marked depletion of myelinated fibers, thin myelin sheaths of the preserved myelinated fibers, and onion bulb formations (2, 3). Ten distinct mutations in *NDRG1* have been identified as genetic defects causing CMT4D (4–11). Among them, the nonsense mutation p.P148X is the most common, suggesting that the loss of NDRG1 function is the leading cause of CMT4D pathogenesis.

NDRG1 is highly expressed in the peripheral nerve system. In myelinated Schwann cells, high phosphorylated NDRG1 is localized to the abaxonal cytoplasm (12). NDRG1 plays diverse roles, including vesicular transport (13, 14), lipid metabolism (15, 16), and cell differentiation and proliferation (17). The most important phenotype induced by NDRG1 deficiency is demyelinating neuropathy (14, 18). Still, how *NDRG1* mutations

lead to CMT4D is unclear, and no effective treatment is available to stop the progression of this debilitating disease. Although a few CMT4D animal models have been generated, neither model fully replicates the features of CMT4D (14, 18, 19).

The myelination of axons in the peripheral nervous system critically depends on the communication between axons and Schwann cells. Neuregulin 1/ErbB signaling has emerged as a major mechanism mediating axon-Schwann cell communication (20). When axonal neuregulin 1 binds to the ErbB3 receptor, it promotes ErbB2-mediated phosphorylation of tyrosine residues in the cytoplasmic domain of both ErbB2 and ErbB3 in Schwann cells. The activation of the ErbB2/3 receptors leads to intracellular signaling through multiple cascades associated with myelination, including AKT, ERK, and JNK (21). Consequently, decreased expression of neuregulin 1 or conditional knockout of ErbB2 in Schwann cells leads to fiber hypomyelination. In addition, neuregulin 1/ErbB signaling is altered in the sciatic nerve of patients with CMT1A presenting a duplication of the *PMP22* gene (22, 23). Significantly, genetic overexpression of neuregulin 1 overcomes impaired nerve development in the CMT1A rat model (24, 25). These studies indicate that the dysregulation of neuregulin 1/ErbB signaling may play an important role in the demyelinating form of CMT. However, no studies have been performed to elucidate the role of neuregulin 1/ErbB signaling in fiber demyelination associated with CMT4D.

In the present study, a novel *Ndrg1*-deficient mouse model was generated. It develops early-onset and progressive demyelinating neuropathy. In *Ndrg1*-deficient mice, although the expression levels of neuregulin 1 and ErbB2/3 were significantly increased, the levels of phosphorated ErbB2/3 and its downstream signaling cascades were decreased. Taken together, our data suggest that the demyelinating phenotype of CMT4D disease is at least partially a consequence of molecular defects in neuregulin 1/ErbB signaling.

RESULTS

***Ndrg1*-deficient mice display early-onset impairments in motor performance.** *Ndrg1*-deficient mice were obtained using CRISPR/Cas9-mediated gene editing (Fig. 1A). The mutation status was validated by sequencing the murine *Ndrg1* gene. We detected NDRG1 expression in the sciatic nerve and found that the protein level was significantly reduced in $Ndrg1^{+/-}$ mice and the protein was not expressed in $Ndrg1^{-/-}$ mice (Fig. 1B). *Ndrg1*-deficient mice were born normally at the expected Mendelian frequencies, indicating that knockout of the *Ndrg1* gene does not cause embryonic death. In addition, $Ndrg1^{-/-}$ mice had a lower body weight than wild-type (WT) mice, especially male mice (Fig. 1C and D). No obvious tumor formation was observed in the *Ndrg1*-deficient mice, although previous studies have found that the downregulation of NDRG1 is associated with tumorigenesis (26).

Our previous report shows that lower limb weakness and abnormal gait are the first symptoms experienced by most patients with CMT4D (8). Here, mice were induced to spread their hind limbs and digits to determine whether the mice lacking *Ndrg1* reproduce CMT4D-like phenotypes. When lifted by the tail, WT and $Ndrg1^{+/-}$ mice spread both hind limbs and all digits of the hind limb paws. In contrast, $Ndrg1^{-/-}$ mice could not spread their hind limbs, suggesting limb muscle weakness (Fig. 1E and F). Subsequent footprint tests revealed gait abnormalities in $Ndrg1^{-/-}$ mice, especially in the stride length (SL) and toe spreading (TS) parameters (Fig. 1G to K). Then, motor balance and coordination were assessed with a rotarod apparatus. Compared with WT and $Ndrg1^{+/-}$ mice, $Ndrg1^{-/-}$ mice had a decreased latency to fall from the rotarod beginning at the age of 4 weeks (Fig. 1L and M). No significant differences in performance on behavior tests were observed between WT and $Ndrg1^{+/-}$ mice at different time points. Signs of motor deficits in $Ndrg1^{-/-}$ mice were observable as early as 4 weeks and were exacerbated with aging. The electrophysiological analysis of the sciatic nerve showed a significantly decreased motor nerve conduction velocity in $Ndrg1^{-/-}$ mice (Fig. 1O). Moreover, amplitudes of compound muscle action potentials were also
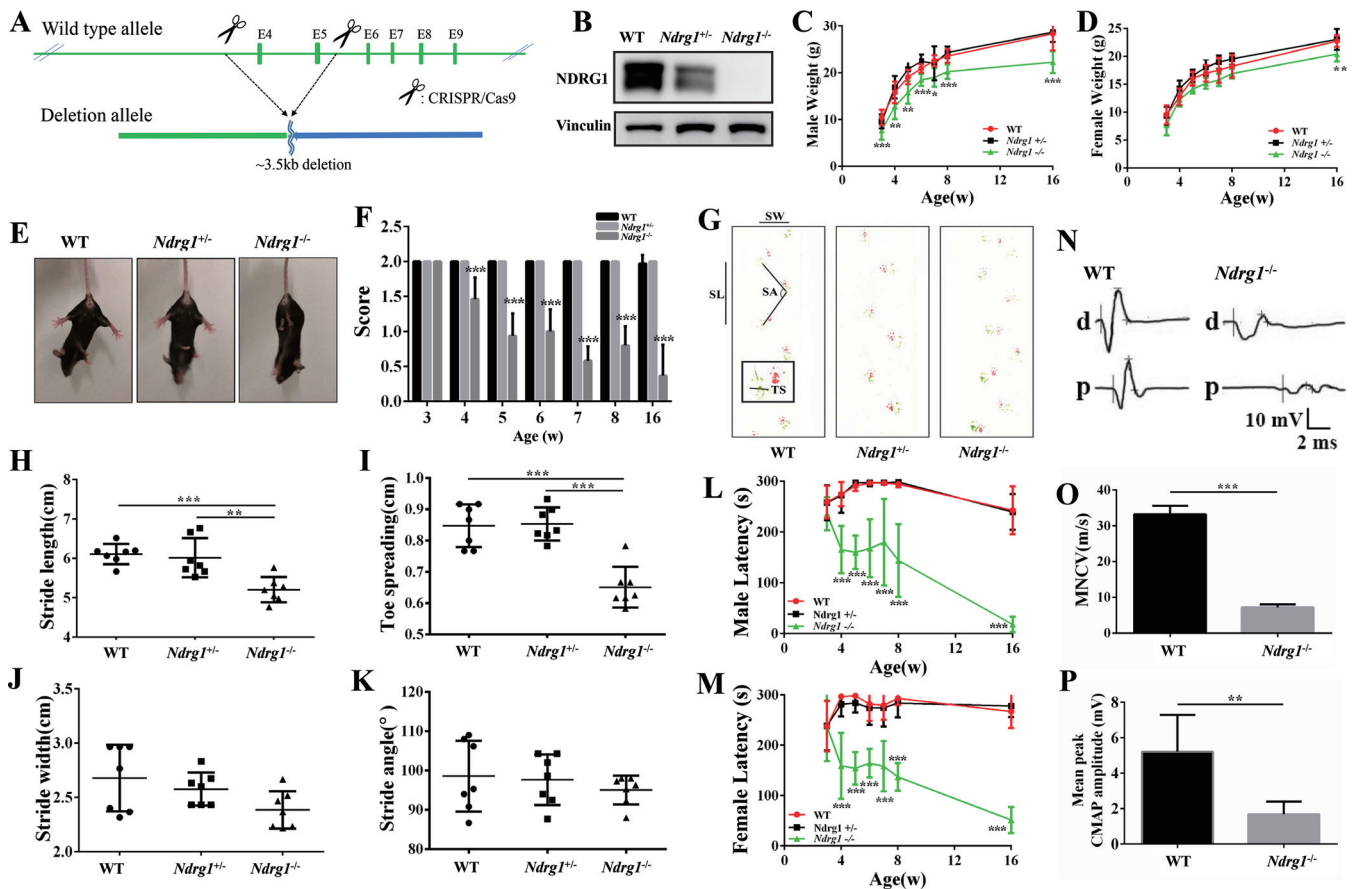
FIG 1 *Ndrg1*-deficient mice develop progressive motor defects. (A) Schematic illustration of the strategy used to construct *Ndrg1*-deficient mice; (B) NDRG1 protein expression in sciatic nerves from 3-week-old WT, *Ndrg1*$^{+/-}$, and *Ndrg1*$^{-/-}$ mice; (C and D) differences in body weight between mice of the three genotypes (male, $n = 7$ per group; female, $n = 6$ per group); (E) hind limb extension test of WT, *Ndrg1*$^{+/-}$, and *Ndrg1*$^{-/-}$ mice. Mice lifted by the tail showed normal spreading of the limbs (WT and *Ndrg1*$^{+/-}$ mice) or limb-clasping behavior (*Ndrg1*$^{-/-}$ mice). (F) *Ndrg1*$^{-/-}$ mice exhibited hind limb weakness with significantly lower scores ($n = 13$ per group). (G) Footprints of WT, *Ndrg1*$^{+/-}$, and *Ndrg1*$^{-/-}$ mice where the stride length (SL), toe spreading (TS), stride width (SW), and stride angle (SA) are depicted. Red represents the forelimbs. Green represents the hind limbs. *Ndrg1*$^{-/-}$ mice exhibited a disrupted walking pattern. (H to K) Quantification of various parameters, including stride length, toe spreading, stride width, and stride angle, obtained from the gait analysis of WT, *Ndrg1*$^{+/-}$, and *Ndrg1*$^{-/-}$ mice ($n = 7$ per group). (L and M) The obviously reduced latency of male and female *Ndrg1*$^{-/-}$ mice on the rotarod began at the age of 4 weeks (male, $n = 7$ per group; female, $n = 6$ per group). (N) An electrophysiological analysis was performed on 8-week-old animals. (O and P) Quantification of motor nerve conduction velocity (MNCV) and compound muscle action potential (CMAP) shows a significant decrease in 8-week-old *Ndrg1*$^{-/-}$ mice ($n = 5$ per group). Data are presented as the mean ± SD. *, $P < 0.05$; **, $P < 0.01$; ***, $P < 0.001$.

reduced (Fig. 1P). These results indicate that the loss of NDRG1 leads to age-dependent motor dysfunction.

Ndrg1-deficient mice show demyelinated neuropathy. To determine whether motor dysfunction in *Ndrg1*$^{-/-}$ mice was due to peripheral nerve demyelination, we performed a light microscopic examination of semithin sections of sciatic nerves isolated from animals aged 2, 4, 8, and 12 weeks. The degeneration of myelin sheaths in *Ndrg1*$^{-/-}$ mice began at 4 weeks of age and was severe at 12 weeks of age (Fig. 2A). We further examined ultrathin sections of the sciatic nerve using a transmission electron microscope to evaluate changes in myelination or the axonal structure. At 2 weeks, *Ndrg1*$^{-/-}$ nerves were similar to those from control animals (Fig. 2B). Neither myelin thickness nor the number of myelinated axons in the sciatic nerve was significantly altered. *Ndrg1*$^{-/-}$ mice began to show thinning of the myelin sheath at the age of 4 weeks, when fiber myelination was normally complete. This provides a window of opportunity for treatment intervention. The occasional onion bulb, axons without myelination, excess collagen deposition, and infiltration of macrophages were observed in *Ndrg1*$^{-/-}$ mice. No abnormalities were observed in WT and *Ndrg1*$^{+/-}$ mice. Older *Ndrg1*$^{-/-}$ mice exhibited more severe demyelination of their sciatic nerves, indicating progressive nerve degeneration. Quantitative analysis indicated that the G ratio of the
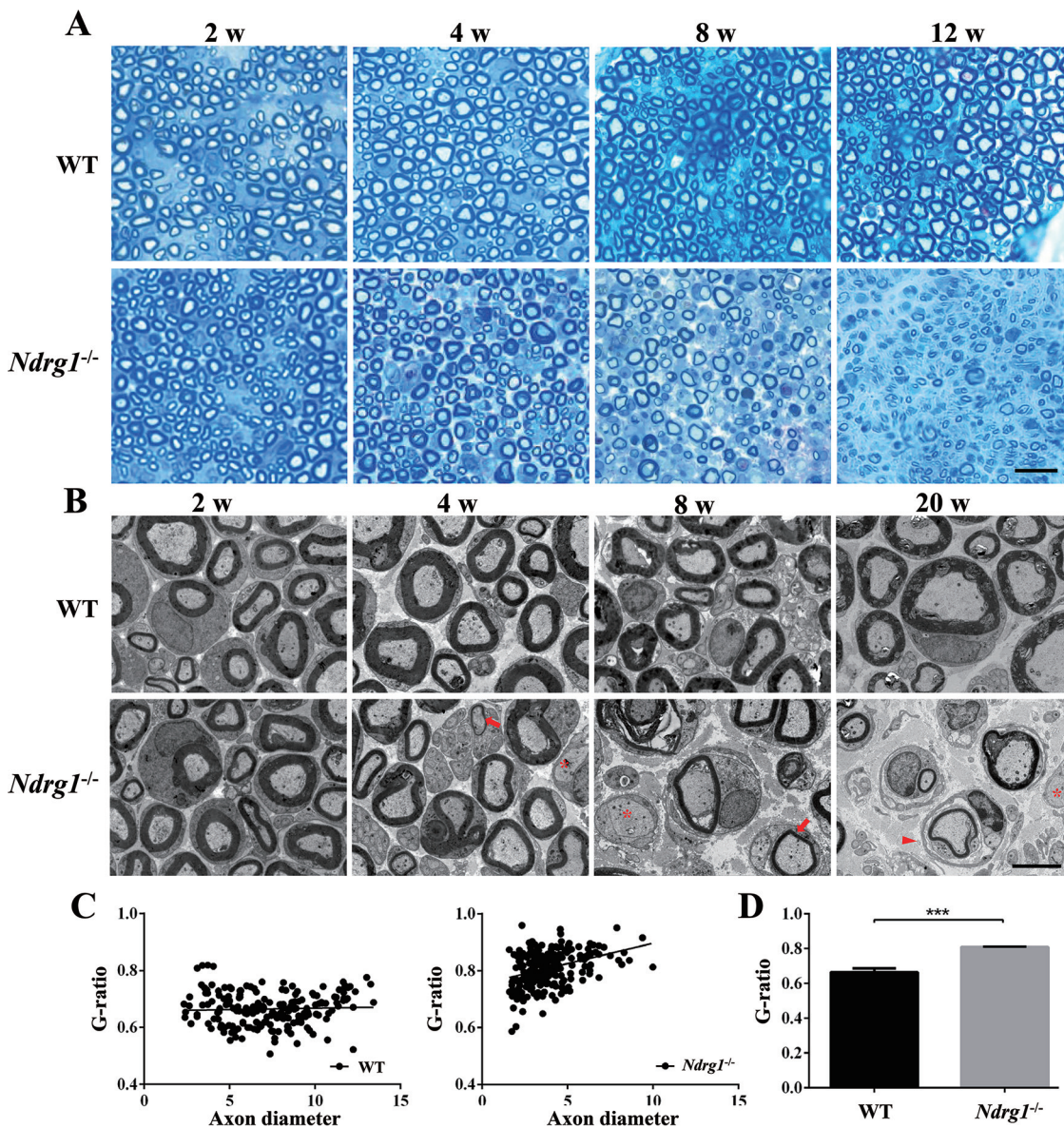
FIG 2 Hypomyelination of the sciatic nerve in *Ndrg1*-deficient mice. (A) Semithin cross sections of sciatic nerves harvested from WT and *Ndrg1$^{-/-}$* mice at different ages were stained with toluidine blue. *Ndrg1$^{-/-}$* mice showed progressive demyelinating neuropathy. (B) Transmission electron micrographs of sciatic nerve cross sections from WT and *Ndrg1$^{-/-}$* mice at different ages. The *Ndrg1$^{-/-}$* mice clearly showed thinly myelinated (arrow) and demyelinated axons (asterisk) at 4 weeks old. The occasional onion bulb (arrowhead) was observed in 20-week-old *Ndrg1$^{-/-}$* mice. (C) Scatterplots of the G ratio (calculated by dividing the axon diameter by the fiber diameter) in 20-week-old animals. (D) The G ratio was higher in *Ndrg1$^{-/-}$* mice than in WT mice ($n = 3$ mice per group; around 56 to 81 fibers per animal were measured). Bars, 10 μm (A) or 5 μm (B). ***, $P < 0.001$.

nerve fibers was significantly increased in *Ndrg1$^{-/-}$* mice, suggesting the presence of demyelinating neuropathy (Fig. 2C and D). Although a shift in the axonal size distribution was observed in *Ndrg1$^{-/-}$* mice, the hypomyelination did not lead to apparent axonal loss (Fig. 2C), suggesting that this model does not completely recapitulate the disease phenotype in CMT4D patients (2, 3). Overall, *Ndrg1$^{-/-}$* mice anatomically and functionally develop early peripheral neuropathy with obvious signs of motor impairment and nerve demyelination.

Ndrg1-deficient mice have abnormal expression patterns of myelination-related proteins. We analyzed the expression level of NDRG1 in various WT mouse tissues to explore the mechanism of peripheral nerve demyelination caused by *Ndrg1* deficiency. NDRG1 was expressed at the highest levels in the sciatic nerve, followed by the spinal cord, and at a lower level in the brain and kidney (Fig. 3A). In the sciatic
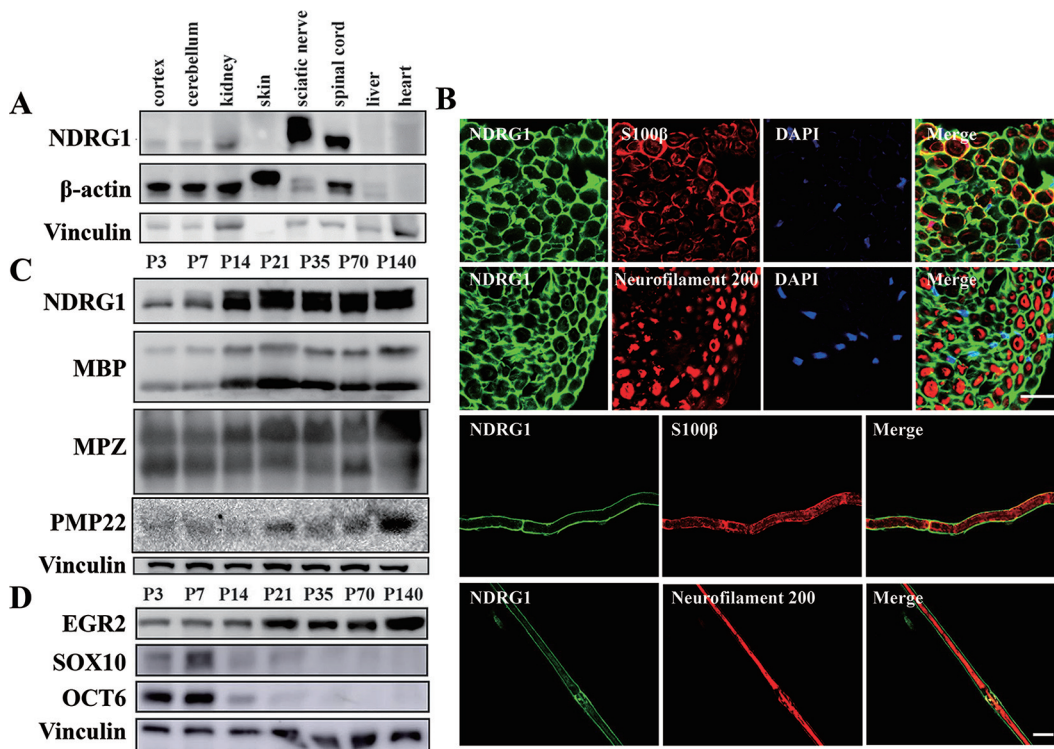
FIG 3 Temporal and spatial distribution of the NDRG1 protein in WT mice. (A) Expression levels of the NDRG1 protein in different tissues from 8-week-old WT mice. The highest NDRG1 level was detected in the sciatic nerve. (B and C) Expression levels of NDRG1, myelin proteins (MBP, MPZ, and PMP22), and transcription factors (EGR2, SOX10, and OCT6) in the sciatic nerves of mice at different postnatal (P) ages (days). (D) Immunofluorescence staining of the sciatic nerve indicated that NDRG1 was expressed in S100β-positive Schwann cells but not in neurofilament 200-positive axons. Bars, 20 μm.

nerve, NDRG1 was restricted to S100β-positive Schwann cells but not detected in neurofilament 200-positive axons (Fig. 3B). Moreover, NDRG1 was expressed at a low level before 2 weeks of age and at a high level after 2 weeks of age. This temporal expression pattern was similar to the myelin proteins (MPZ, MBP, and PMP22) required for nerve myelination (Fig. 3C).

Next, we explored the effect of *Nrdg1* deletion on the expression levels of myelin proteins and transcription factors in the sciatic nerve. Compared with WT mice, the mRNA and protein levels of MBP and MPZ proteins were reduced in *Ndrg1*$^{-/-}$ mice (Fig. 4A to C). Intriguingly, the *Pmp22* mRNA level was decreased in *Ndrg1*$^{-/-}$ mice (Fig. 4C), while the PMP22 protein level was significantly increased (Fig. 4A and B), suggesting that *Ndrg1* deletion may affect the degradation of PMP22 protein. We then detected the protein levels of EGR2, SOX10 and OCT6 in WT and *Ndrg1*$^{-/-}$ mice of different ages. These transcription factors are required for nerve myelination (27). In the sciatic nerve of *Ndrg1*$^{-/-}$ mice, EGR2 levels were decreased at all ages, OCT6 levels were increased at 4, 10, and 20 weeks, and SOX10 levels were decreased at 2, 4, and 10 weeks but increased at 20 weeks (Fig. 4D to G). In summary, the demyelinated neuropathy in *Ndrg1*$^{-/-}$ mice is accompanied by an abnormal expression pattern of myelination-related proteins.

Ndrg1 deficiency impairs neuregulin 1/ErbB signaling. Given the critical role of the ErbB2/3 in fiber myelination (20), we investigate whether the activation of these kinases might be altered in *Ndrg1*-deficient mice at different developmental stages. Compared with WT mice, the level of total ErbB3 receptor was increased at any of the stages tested (beginning at 2 weeks), while the amount of total ErbB2 receptor was significantly increased at 4 weeks and thereafter in *Ndrg1*$^{-/-}$ mice (Fig. 5A and B). However, the relative levels of the activated (phosphorylated) forms of the two coreceptors ErbB2 and ErbB3 were significantly decreased in *Ndrg1*-deficient nerves
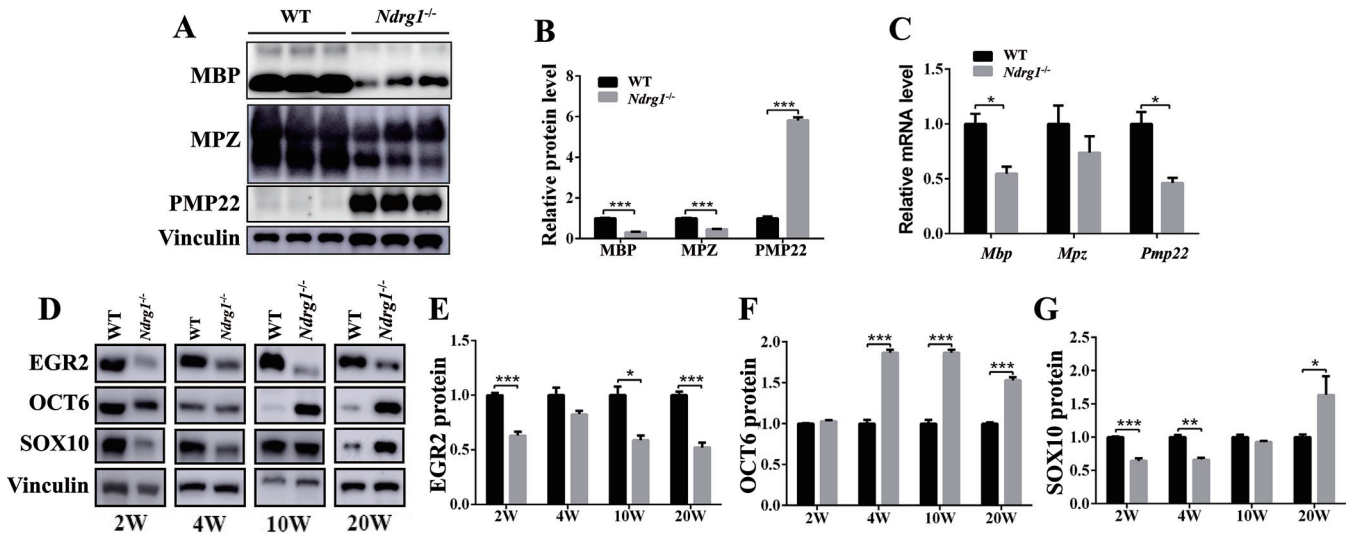
FIG 4 *Ndrg1*-deficient mice displayed an abnormal expression pattern of myelination-related proteins in the sciatic nerve. (A) Western blot analysis of MBP, MPZ, and PMP22 protein levels in the sciatic nerves from 20-week-old WT and *Ndrg1*$^{-/-}$ mice. (B) Quantification of band intensities shows an increased level of PMP22 and decreased MBP and MPZ in the sciatic nerves ($n = 3$ per group). (C) Real-time PCR analysis showed significantly decreased *Mbp* and *Pmp22* mRNA levels in sciatic nerve from 20-week-old *Ndrg1*$^{-/-}$ mice ($n = 3$ per group). (D) Western blot analysis of EGR2, OCT6, and SOX10 protein levels in the sciatic nerves from WT and *Ndrg1*$^{-/-}$ mice at different ages; (E to G) quantification of EGR2, OCT6, and SOX10 protein levels in the sciatic nerves from WT and *Ndrg1*$^{-/-}$ mice at different ages ($n = 3$ per group). Data are presented as the means ± SEM. *, $P < 0.05$; ***, $P < 0.001$.

(Fig. 5D and F). To further evaluate the potential cellular consequences of the observed changes, we analyzed the activation of some of their downstream signaling cascades that play vital roles in Schwann cell myelination. Compared to WT mice, the relative levels of phosphorylated AKT, extracellular signal-regulated kinase (ERK), and Jun N-terminal protein kinase (JNK) were decreased in *Ndrg1*$^{-/-}$ mice. This decrease was more obvious at 20 weeks (Fig. 5G to I). These findings suggest that the ErbB2/3 mediating signaling was impaired in the *Ndrg1*$^{-/-}$ nerve.

Neuregulin 1 binds to ErbB2/3 receptors on the membrane of Schwann cells and promotes the phosphorylation of ErbB2/3 (20). However, the decreased phosphorylation of ErbB2/3 in *Ndrg1*$^{-/-}$ mice was not associated with changes in the level of the neuregulin 1 ligand, which was significantly increased at 4 weeks and thereafter (Fig. 5A and J). In addition, we found that the level of integrin β4 (ITGB4), a receptor also mainly located on Schwann cells, was significantly decreased in the absence of NDRG1 (Fig. 6A to C). It has been demonstrated that ITGB4 positively regulates neuregulin 1/ErbB signaling (28, 29). The decreased ITGB4 may reduce ErbB2 phosphorylation and impair ErbB2-mediating signaling (30, 31). Subsequent *in vitro* experiments showed that silencing endogenous *NDRG1* in cells decreased the level of ITGB4 and phosphorylated ERK, while NDRG1 overexpression increased the level of ITGB4 and phosphorylated ERK (Fig. 6D and E). Taken together, *Ndrg1* deletion results in the dysregulation of neuregulin 1/ErbB signaling. Abnormal neuregulin 1/ErbB signaling to downstream targets may partially contribute to the demyelination observed in *Ndrg1*-deficient mice.

DISCUSSION

With the development of next-generation sequencing technology, genetic studies have documented new CMT4D cases during the last decade (4–6, 10). Although the identification of *NDRG1* as the gene that is mutated in patients with CMT4D led to a substantially improved clinical diagnosis in the affected families, the functional role of NDRG1 in peripheral nerves remains unknown. Here, we describe the generation and analysis of a new mouse model of CMT4D disease that led to discovery of a role for NDRG1 in peripheral nerve myelination.

Pathological findings in patients with CMT4D generally reveal a marked reduction in the number of myelinated fibers. The remaining fibers have relatively thin myelin sheaths.
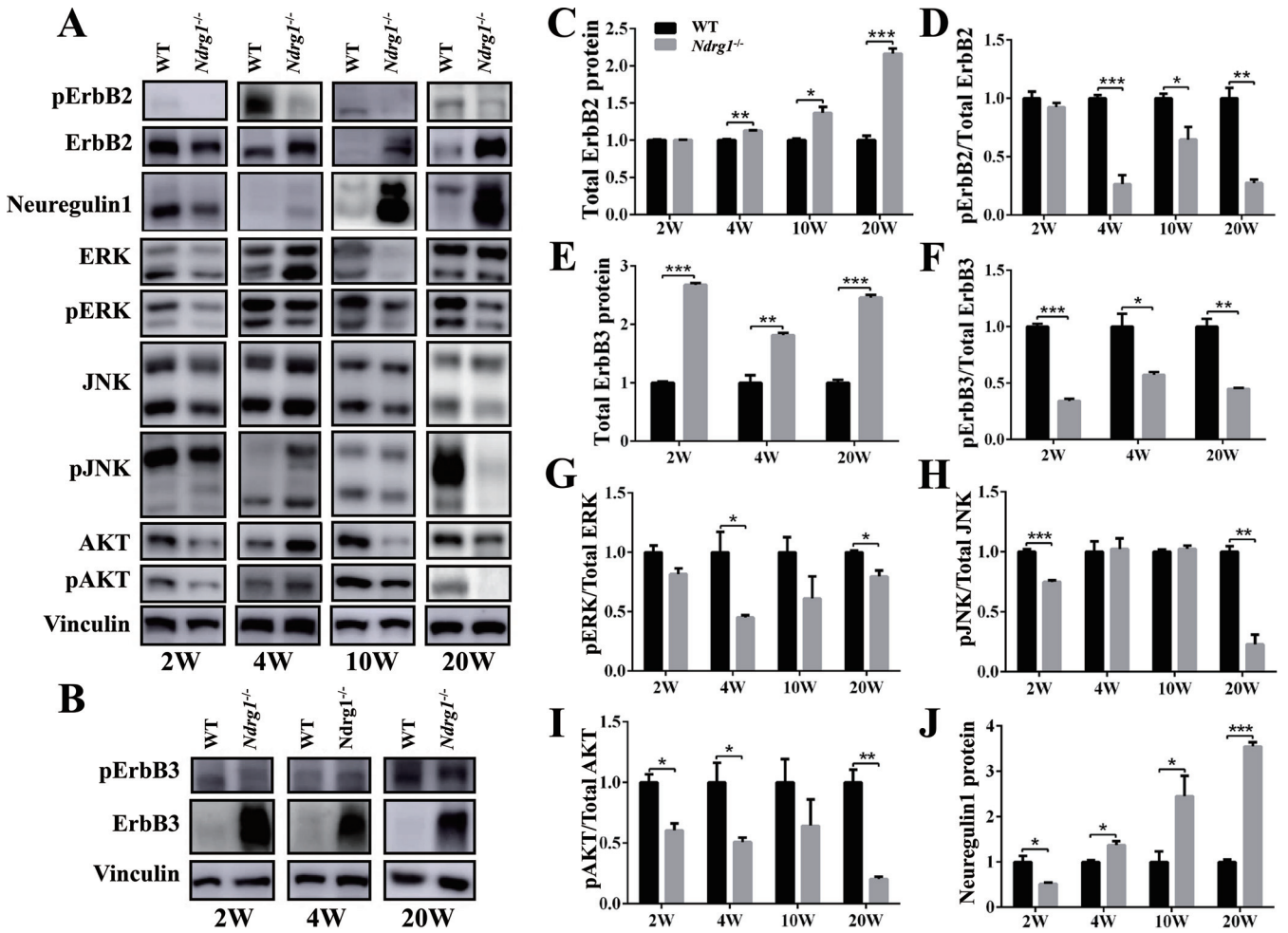
FIG 5 Neuregulin1/ErbB signaling was dysregulated in *Ndrg1*-deficient mice. (A) Western blot images showing levels of ErbB2, ERK, AKT, JNK, and their phosphorylated forms in the sciatic nerves from both WT and *Ndrg1$^{-/-}$* mice at different ages. (B) Western blot images show ErbB3 and phosphorylated ErbB3 protein levels in the sciatic nerves from WT and *Ndrg1$^{-/-}$* mice. (B and C) The level of total ErbB2 protein was significantly increased in the sciatic nerves from *Ndrg1$^{-/-}$* mice at 4 weeks, 10 weeks, and 20 weeks (*n* = 3 per group). (D) The ratio of phosphorylated ErbB2 to total ErbB2 was significantly decreased in the sciatic nerves from *Ndrg1$^{-/-}$* mice at 4 weeks, 10 weeks, and 20 weeks (*n* = 3 per group). (E) The level of total ErbB3 protein was significantly increased in the sciatic nerves from *Ndrg1$^{-/-}$* mice at 2 weeks, 4 weeks, and 20 weeks (*n* = 3 per group). (F) The ratio of phosphorylated ErbB3 to total ErbB3 was significantly decreased in the sciatic nerves from *Ndrg1$^{-/-}$* mice at 2 weeks, 4 weeks, and 20 weeks (*n* = 3 per group). (G to I) The activation of downstream targets of ErbB2/3 (ERK, AKT, and JNK) was assessed by immunoblotting sciatic nerve extracts and quantifying the relative levels of phosphorylated forms compared to total protein levels (*n* = 3 per group). (J) Compared with WT mice, *Ndrg1$^{-/-}$* mice exhibited higher levels of neuregulin 1 beginning at 4 weeks (*n* = 3 per group). *, $P < 0.05$; **, $P < 0.01$; ***, $P < 0.001$.

Multiple onion bulb formations were also observed in nerve samples from young patients with CMT4D (32). In this study, we generated a novel mouse model of CMT4D disease with a deletion of exons 4 to 5 in the *Ndrg1* gene. This mutation results in undetectable levels of the NDRG1 protein in the sciatic nerve. Mice lacking this gene develop progressive demyelination. Nerve conduction velocity measurements, morphometric analyses, and motor performance indicated the presence of neuropathy at 4 weeks of age, suggesting an early onset of the disease in *Ndrg1*-deficient mice. However, this model did not capture all the features of CMT4D patients. The mice did not display early severe axonal loss, and only occasional minor onion bulb changes were found at later stages. This interspecies phenotypic variation in NDRG1 mutants may be related to their genetic backgrounds (14, 19).

Compared to the previously reported CMT4D models, namely, hypomorphic *Ndrg1* knockout (KO) mice and *stretcher* (*str*) mice, our *Ndrg1*-deficient mice displayed an earlier onset of motor impairment (14, 18). Given the recessive pattern of inheritance and the lack of manifestations in heterozygous carriers, the likely explanation for this difference is the total lack of a functional NDRG1 protein. The *Ndrg1* gene contains 16 exons.
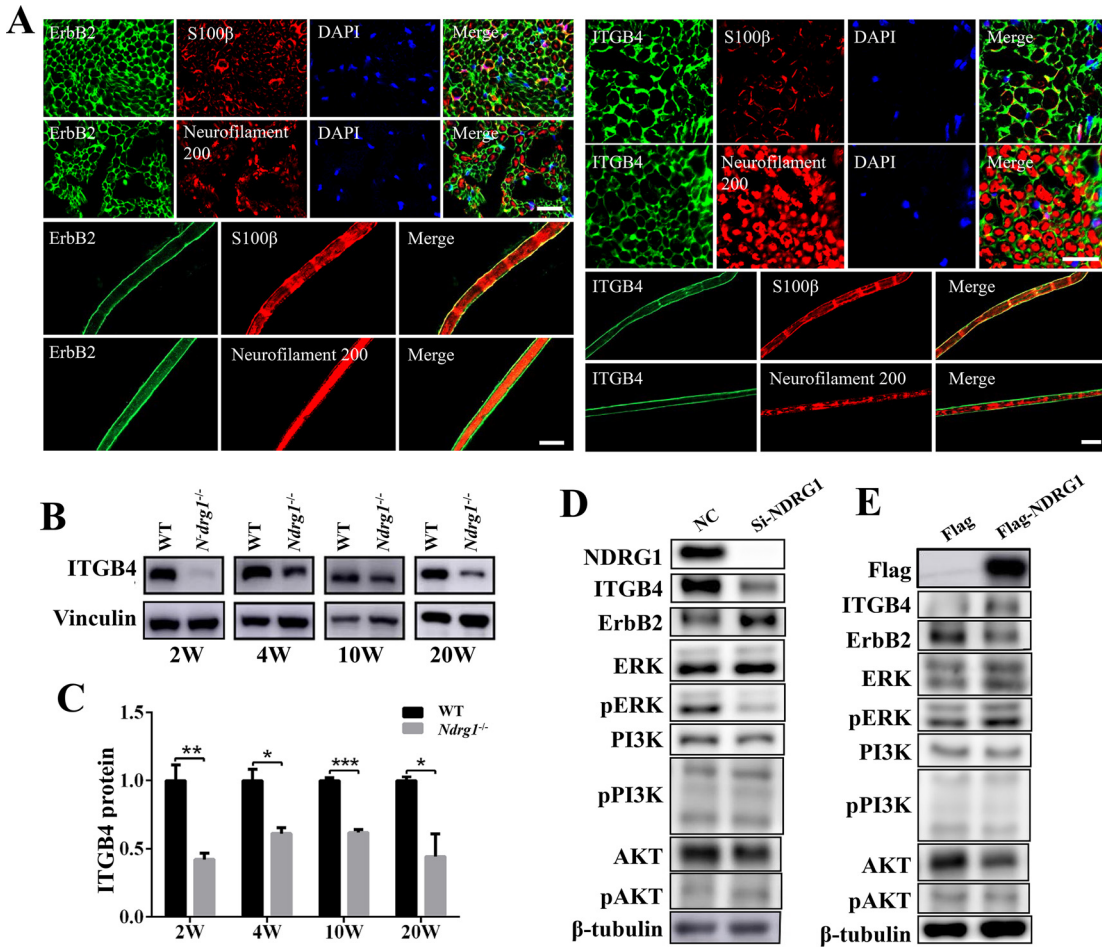
FIG 6 *Ndrg1*-deficient mice show decreased ITGB4 in sciatic nerves. (A) The immunofluorescence staining of the sciatic nerve of WT mice indicated that ErbB2 and ITGB4 were expressed in the S100β-positive Schwann cell rather than neurofilament 200-positive axon. Bars, 20 μm. (B) Western blot images of ITGB4 protein in sciatic nerves from WT and *Ndrg1*$^{-/-}$ mice at different ages. (C) The level of ITGB4 protein was significantly decreased in sciatic nerves from *Ndrg1*$^{-/-}$ mice (n = 3 per group). (D) The endogenous NDRG1 in the A549 cell was knocked down via siRNA. The negative-control (NC) group was transfected with scrambled siRNA. Western blot analysis showed decreased ITGB4 and phosphorylated ERK in NDRG1 knockdown cells. (E) The plasmids expressing Flag-NDRG1 or Flag were transiently transfected in A549 cells. Western blot analysis showed increased ITGB4 and phosphorylated ERK in NDRG1-overexpressing cells. Data are presented as the mean ± SEM. *, $P < 0.05$; **, $P < 0.01$; ***, $P < 0.001$.

The fourth and fifth exons of the *Ndrg1* gene were deleted in our *Ndrg1*-deficient mice to form a protein fragment with a length of only 33 amino acids. This fragment did not contain any functional domain, such as a catalytic site, metal ion binding site, or phosphorylation site (33). However, low leaky expression of NDRG1 was detected in *Ndrg1* KO mouse, and a mutant protein missing the 99 amino acids encoded by the deleted exons was observed in *str* mouse (14, 18). Taken together, our findings further support the hypothesis that even very low levels of the functional NDRG1 protein lead to a significantly milder phenotype of CMT4D.

The formation and maintenance of the nerve myelin sheath are strictly regulated by transcription factors. SOX10, OCT6, and ERG2 are the core transcription factors involved in regulating the expression of a large number of myelin genes (34, 35). Our results revealed that the temporal expression pattern of the NDRG1 protein is correlated with the expression of the aforementioned transcription factors. Compared with WT animals, *Ndrg1*-deficient mice displayed abnormal expression patterns of these transcription factors, accompanied by decreased mRNA levels of myelin genes. Thus, the demyelination of peripheral nerves caused by *Ndrg1* deficiency may be partially attributed to abnormal transcriptional regulation in Schwann cells. Interestingly, the

level of PMP22, which is primarily expressed in the compact myelin of the peripheral nervous system, was significantly increased in *Ndrg1*-deficient mice. Several rodent studies have shown that PMP22 overexpression is sufficient to cause a demyelinating neuropathy (36). Further studies are necessary to clarify the mechanism underlying the increase in PMP22 protein levels caused by *Ndrg1* deletion.

Neuregulin1/ErbB signaling plays a major role in controlling axon-Schwann cell communication. Recent studies have revealed that several demyelinating CMT-linked proteins, such as SH3TC2 and SIMPLE, are novel regulators of endocytic trafficking that may affect neuregulin 1/ErbB signaling (21, 37). In our *Ndrg1*-deficient mice, the phosphorylated ErbB2 and ErbB3 receptors and their downstream signaling proteins were significantly decreased, indicating impaired neuregulin 1/ErbB signaling. These studies further support the hypothesis that dysregulation of neuregulin 1/ErbB signaling in Schwann cells may represent a common pathogenic mechanism in multiple subtypes of demyelinating CMT (21).

Currently, ErbB2/3 receptor signaling is presumed to be regulated by endocytic trafficking, which controls the intracellular distribution and degradation of ErbB receptors (21). NDRG1 is considered a regulator of endosomal trafficking (8, 38). It functions as a Rab4a effector localized to endosomes (38). The deletion of NDRG1 impairs the endosomal sorting complex required for the transport (ESCRT) system, causing the low-density lipoprotein receptor (LDLR) to accumulate in abnormally enlarged endosomes (16). Our previous study also showed that the Rab4a-positive endosome was enlarged in NDRG1 knockdown cells (8). Taken together, the dysfunction of neuregulin 1/ErbB signaling in *Ndrg1*-deficient sciatic nerves may be associated with impaired trafficking of ErbB receptors in Schwann cells. Further studies will be required to clarify this issue. In addition, we found that the level of ITGB4 was significantly decreased in *Ndrg1*-deficient mice. ITGB4 is a receptor localized in the Schwann cell. It has been demonstrated that ITGB4 interacts with ErbB2/3 and enhances the neuregulin 1/ErbB signaling (28, 29, 39). Reduced ITGB4 may contribute to the impaired neuregulin 1/ErbB signaling in *Ndrg1*-deficient mice.

According to recent studies, upregulation of neuregulin 1 in a CMT1A rat model during the early postnatal period effectively alleviates peripheral nerve demyelination and restores axon survival into adulthood (24). In addition, genetic overexpression of neuregulin 1 ameliorates altered neurophysiological and morphological parameters in a mouse model of demyelinating CMT1B (25). These studies suggest that the upregulation of neuregulin 1 may be an effective treatment to rescue demyelination. However, it was also found that downregulation of neuregulin 1 signaling via niacin (Niaspan) treatment ameliorates neuropathy in a mouse model of demyelinating CMT4B1 (40). In this report, we observed increased expression of neuregulin 1 in *Ndrg1*-deficient mice, consistent with the results observed in a rat model of CMT1A (23). Moreover, although neuregulin 1 expression was increased, expression of the activated ErbB receptor was decreased in *Ndrg1*-deficient mice. Therefore, considering the impaired trafficking of ErbB receptors in Schwann cells in demyelinating CMT (21, 27), a therapeutic approach based on neuregulin 1 treatment should be carefully reconsidered.

In summary, NDRG1 is essential for proper myelination by Schwann cells. Our description of *Ndrg1*-deficient mice indicated that these animals replicate the progressive demyelination phenotype of CMT4D. Furthermore, the dysregulation of neuregulin 1/ErbB signaling may be involved in demyelinated neuropathy in CMT4D disease. Therefore, modulation of the neuregulin 1/ErbB signaling may be a potential therapeutic strategy to alleviate CMT4D neuropathy.

MATERIALS AND METHODS

Animal and PCR genotyping. $Ndrg1^{-/-}$ mice were generated with the CRISPR/Cas9 system as reported previously (41). Briefly, two different single-guide RNAs (sgRNA5, GGGCCAACAACTTCCCA TTCTGG; sgRNA14, GTGTGACACCCCTTGTCTTGGGG) targeting intron 3–4 and intron 5–6 of the *Ndrg1* gene were used to generate mutations that make protein translation stop prematurely. Subsequently, mixtures of sgRNAs and *Cas9* mRNA were microinjected into fertilized embryos of C57BL/6N mice (Biocytogen). Mutations in *Ndrg1* were confirmed by Sanger sequencing analyses. The mice used in this

study were obtained from $Ndrg1^{+/-}$ self-crossed inbred mice. Mice were maintained under specific-pathogen-free conditions on a 12-h light/dark cycle and had free access to water and diet. Mouse genomic DNA was isolated from tail biopsy samples and extracted with a DNA purification kit (Tsingke Biotechnology). Primers F (5′-CTGAGGACTCGGAACGAAGGTGAAG-3′) and Rwt (5′-ACCTAGCAATGTTT AACTAGCAGCCA-3′) were used to characterize the wild-type (WT) allele, and primers F and Rmt (5′-GAAAGGAGGGGCAAAGACATGGGAC-3′) were used to detect the mutated allele. All procedures involving the use of animals were conducted following the approved guidelines of the Institutional Animal Care and Use Committee of Tongji University. Unless indicated otherwise, only male mice were used in this study.

Hind limb extension test. Mice performed the hind limb extension test at different ages using a previously reported method (42). Mice were suspended by the tail, and the extent of hind limb extension was observed over 10 s. A score of 2 corresponded to a normal extension reflex in hind limbs with splaying of toes. A score of 1 corresponded to clenching of hind limbs to the body with partial splaying of toes. A score of 0 corresponded to clasping hind limbs with curled toes. A score of 1.5 or 0.5 corresponded to behavior between 2 and 1 or between 1 and 0, respectively. Three tests were performed for each mouse at 30-s intervals.

Footprint analysis. The footprint was analyzed using a previously reported method (42, 43). The hind paws and forepaws of each mouse were painted with two different nontoxic inks, respectively. Then, the animal was placed in a narrow alley (65 by 5 by 15 cm) with the floor covered with white paper. A dark box was placed at the end of the alley for the animal to walk to while leaving its footprints on the paper. At least three consecutive footprints were used to assess gait characteristics on both sides, including stride length (SL), stride width (SW), stride angle (SA), and the degree of toe spreading (TS). The parameters were averaged for statistical analysis.

Rotarod test. Motor coordination was assessed with a rotarod apparatus as reported previously (43). Mice underwent 3 days of training on a rotarod apparatus at a constant speed of 15 rpm for 3 min or until a fall occurred. For testing, the rotation of the rotarod was accelerated from 0 rpm to 40 rpm. The latency of each mouse to fall was monitored in three consecutive trials, and the intratrial interval for each animal was 30 min. The average latency in the three trials was used as a measure of motor performance.

Electrophysiology. The average motor nerve conduction velocities (MNCVs) and compound muscle action potential (CMAP) of the sciatic nerve were calculated in 8-week-old mice as previously described (14). Briefly, mice were intraperitoneally anesthetized with sodium pentobarbital. Motor nerve conduction was estimated in the sciatic nerve using a Dantec Keypoint electromyograph. Needle electrodes were inserted with the stimulating cathode at the sciatic notch and the ankle; recording electrodes were inserted into the foot muscles. The ground electrode was inserted into the skin on the back.

Western blot. Tissues or cells were homogenized in radioimmunoprecipitation assay (RIPA) buffer with a cocktail of protease inhibitors and phosphatase inhibitors. The concentration was measured with the Pierce bicinchoninic acid (BCA) protein assay kit (Thermo Fisher). The total lysates (30 μg) were loaded in Tris-glycine gel and blotted onto a polyvinylidene difluoride (PVDF) membrane. The membrane was blocked with 5% nonfat dry milk in Tris-buffered saline (TBS) containing 0.1% Tween 20 (TBST) for 1 h at room temperature (RT) and then incubated with specific primary antibodies overnight on a shaker at 4°C. The following antibodies were used: anti-NDRG1 (ab124689; Abcam), anti-vinculin (A14193; Abclonal), anti-β-actin (AC026; Abclonal), anti-Flag (M20008; Abmart), anti-MBP (ab40390; Abcam), anti-MPZ (ab31851; Abcam), anti-PMP22 (sc515199; Santa Cruz Biotechnology), anti-SOX10 (ab155279; Abcam), anti-EGR2 (ab108399; Abcam), anti-OCT6 (ab126746; Abcam), anti-ErbB2 (MA5-13675; Thermo Fisher), anti-pErbB2 (Tyr1248, no. 2247; Cell Signaling Technology), anti-ErbB3 (SC-415; Santa Cruz Biotechnology), anti-pErbB3 (Tyr1289, no. 4791; Cell Signaling Technology), anti-ITGB4 (ab29042; Abcam), anti-ERK (no. 4695; Cell Signaling Technology), anti-pERK (Thr202/Tyr204, no. 4370; Cell Signaling Technology), anti-JNK (no. 9252; Cell Signaling Technology), anti-pJNK (Thr183/Tyr185, no. 9255; Cell Signaling Technology), anti-AKT (Cell Signaling Technology), anti-pAKT (Thr308, no. 4056; Cell Signaling Technology), anti-phosphatidylinositol 3-kinase (anti-PI3K) (no. 4249; Cell Signaling Technology), anti-pPI3K (Tyr458/Tyr199, no. 4228; Cell Signaling Technology), and anti-neuregulin 1 (no. 147724; R&D Systems). After being washed three times in TBST, membranes were incubated with goat anti-rabbit or goat anti-mouse secondary antibody at RT for 1 h. Next, the membranes were washed three times with TBST. Enhanced chemiluminescence (ECL) was then used to visualize the bands. Samples from WT and $Ndrg1^{-/-}$ mice of the same age were run on the same Western blot and quantified. The phosphorylated proteins were quantitatively normalized to total proteins, and the other proteins were quantitatively normalized to vinculin.

Quantitative real-time PCR. Total RNA was extracted from sciatic nerves using TRIzol reagent (Invitrogen) and subjected to reverse transcription via a PrimerScript RT reagent kit (TaKaRa). Quantitative PCR (qPCR) was used for the relative quantitation of *Pmp22*, *Mpz*, and *Mbp* mRNA with AceQ Universal SYBR qPCR master mix (Vazyme). qPCR was performed on a LightCycler 96 instrument (Roche). The cycling conditions were as follows: initial denaturation at 95°C for 5 min followed by 40 cycles at 94°C for 10 s and 60°C for 30 s. All primers were designed to prevent the amplification of genomic DNA. Primer sequences are listed in parentheses: *Pmp22* (5′-ATGGACACACGACTGATCTCT-3′; 5′-CAGCCATTCGCTCACTGATGA-3′), *Mpz* (5′-GTC CAGTGAATGGGTCTCAGATG-3′; 5′-CTTGGCATAGTGGAAAATCGAAA-3′), *Mbp* (5′-TCACAGCGATC CAAGTACC TG-3′; 5′-CCCCTGTCACCGCTAAAGAA-3′), and 18S rRNA (5′-CTCAACACGGGAAACCTCAC-3′; 5′-CGCTCCA CCAACTAAGAACG-3′).

Immunofluorescence staining. Sciatic nerves were dissected and frozen in the OCT (optimal cutting temperature) compound. Sections (10 μm) were washed three times for 5 min each in 0.01 M phosphate-buffered saline (PBS) and then blocked with 5% bovine serum albumin (BSA) in 0.1% Triton X-100 solution in PBS (PBST) for 30 min at RT. Subsequently, sections were incubated with specific primary

antibodies in 5% BSA supplemented with 0.1% PBST at 4°C overnight. The following antibodies were used: anti-NDRG1 (sc398291 from Santa Cruz Biotechnology and ab124689 from Abcam), anti-S100β (ab52642; Abcam), anti-neurofilament 200 (N4142; Sigma), anti-ErbB2 (MA5-13675; Thermo Fisher), and anti-ITGB4 (ab29042; Abcam). Thereafter, sections were washed three times for 5 min with PBS and incubated with secondary antibodies in 5% BSA supplemented with 0.1% PBST for 2 h at RT. After being washed and then incubated with DAPI, sections were visualized under a Nikon confocal microscope.

Morphometric analysis. The middle sciatic nerves were isolated and fixed with 2.5% glutaraldehyde. Semithin sections from mice aged 2 weeks, 4 weeks, 8 weeks, and 12 weeks were stained with toluidine blue and examined under a light microscope. For the transmission electron microscopy analysis, ultrathin sections from mice aged 2 weeks, 4 weeks, 8 weeks, and 20 weeks were stained with uranyl acetate and lead citrate. The ultrathin stained sections were observed with a transmission electron microscope (Hitachi TEM system).

Cell culture and transfection. A549 cells were grown in a culture medium consisting of Dulbecco's modified Eagle's medium (DMEM), 10% fetal bovine serum (Gibco), and 1% penicillin and streptomycin (Invitrogen) in a humidified 5% CO_2 incubator at 37°C. Cells were transfected with the expression vector pFlag-CMV4-NDRG1 or pFlag-CMV4 using Lipofectamine 3000 (Invitrogen) as described in our previously reported study (8). Cells were transfected with a small interfering RNA (siRNA) (sense, 5′-GCGCCUAACUCGG UAUUAATT-3′; antisense, 5′-UUAAUACCGAGUUAGG CGCTT-3′) using Lipofectamine RNAiMAX (Invitrogen) to knock down endogenous NDRG1.

Statistical analysis. Statistical analysis was performed using GraphPad Prism version 6.01. All values are reported as the mean ± standard deviation (SD) or mean ± standard error of the mean (SEM). The data were analyzed using Student's t test or one-way analysis of variance (ANOVA) according to the number of groups compared. Tukey's honestly significant difference (HSD) test was used for *post hoc* analysis. For all analyses, statistical significance is denoted as follows: *, $P < 0.05$; **, $P < 0.01$; ***, $P < 0.001$.

REFERENCES

1. Kalaydjieva L, Gresham D, Gooding R, Heather L, Baas F, de Jonge R, Blechschmidt K, Angelicheva D, Chandler D, Worsley P, Rosenthal A, King RH, Thomas PK. 2000. N-myc downstream-regulated gene 1 is mutated in hereditary motor and sensory neuropathy-Lom. Am J Hum Genet 67: 47–58. https://doi.org/10.1086/302978.

2. Kalaydjieva L, Nikolova A, Turnev I, Petrova J, Hristova A, Ishpekova B, Petkova I, Shmarov A, Stancheva S, Middleton L, Merlini L, Trogu A, Muddle JR, King RH, Thomas PK. 1998. Hereditary motor and sensory neuropathy—Lom, a novel demyelinating neuropathy associated with deafness in gypsies. Clinical, electrophysiological and nerve biopsy findings. Brain 121:399–408. https://doi.org/10.1093/brain/121.3.399.

3. Colomer J, Iturriaga C, Kalaydjieva L, Angelicheva D, King RH, Thomas PK. 2000. Hereditary motor and sensory neuropathy—Lom (HMSNL) in a Spanish family: clinical, electrophysiological, pathological and genetic studies. Neuromuscul Disord 10:578–583. https://doi.org/10.1016/S0960-8966(00)00149-8.

4. Chen B, Niu S, Chen N, Pan H, Wang X, Zhang Z. 2018. A novel homozygous NDRG1 mutation in a Chinese patient with Charcot-Marie-Tooth disease 4D. J Clin Neurosci 53:231–234. https://doi.org/10.1016/j.jocn.2018.04.024.

5. Chen CX, Dong HL, Wei Q, Li LX, Yu H, Li JQ, Liu GL, Li HF, Bai G, Ma H, Wu ZY. 2019. Genetic spectrum and clinical profiles in a southeast Chinese cohort of Charcot-Marie-Tooth disease. Clin Genet 96:439–448. https://doi.org/10.1111/cge.13616.

6. Dohrn MF, Glockle N, Mulahasanovic L, Heller C, Mohr J, Bauer C, Riesch E, Becker A, Battke F, Hortnagel K, Hornemann T, Suriyanarayanan S, Blankenburg M, Schulz JB, Claeys KG, Gess B, Katona I, Ferbert A, Vittore D, Grimm A, Wolking S, Schols L, Lerche H, Korenke GC, Fischer D, Schrank B, Kotzaeridou U, Kurlemann G, Drager B, Schirmacher A, Young P, Schlotter-Weigel B, Biskup S. 2017. Frequent genes in rare diseases: panel-based next generation sequencing to disclose causal mutations in hereditary neuropathies. J Neurochem 143:507–522. https://doi.org/10.1111/jnc.14217.

7. Hunter M, Bernard R, Freitas E, Boyer A, Morar B, Martins IJ, Tournev I, Jordanova A, Guergelcheva V, Ishpekova B, Kremensky I, Nicholson G, Schlotter B, Lochmuller H, Voit T, Colomer J, Thomas PK, Levy N, Kalaydjieva L. 2003. Mutation screening of the N-myc downstream-regulated gene 1 (NDRG1) in patients with Charcot-Marie-Tooth Disease. Hum Mutat 22:129–135. https://doi.org/10.1002/humu.10240.

8. Li LX, Liu GL, Liu ZJ, Lu C, Wu ZY. 2017. Identification and functional characterization of two missense mutations in NDRG1 associated with Charcot-Marie-Tooth disease type 4D. Hum Mutat 38:1569–1578. https://doi.org/10.1002/humu.23309.

9. Okamoto Y, Goksungur MT, Pehlivan D, Beck CR, Gonzaga-Jauregui C, Muzny DM, Atik MM, Carvalho CMB, Matur Z, Bayraktar S, Boone PM, Akyuz K, Gibbs RA, Battaloglu E, Parman Y, Lupski JR. 2014. Exonic duplication CNV of NDRG1 associated with autosomal-recessive HMSN-Lom/CMT4D. Genet Med 16:386–394. https://doi.org/10.1038/gim.2013.155.

10. Piscosquito G, Magri S, Saveri P, Milani M, Ciano C, Farina L, Taroni F, Pareyson D. 2017. A novel NDRG1 mutation in a non-Romani patient with CMT4D/HMSN-Lom. J Peripher Nerv Syst 22:47–50. https://doi.org/10.1111/jns.12201.

11. Pravinbabu P, Holla VV, Phulpagar P, Kamble N, Netravathi M, Yadav R, Pal PK, Muthusamy B. 2022. A splice altering variant in NDRG1 gene causes Charcot-Marie-Tooth disease, type 4D. Neurol Sci https://doi.org/10.1007/s10072-022-05893-4.

12. Heller BA, Ghidinelli M, Voelkl J, Einheber S, Smith R, Grund E, Morahan G, Chandler D, Kalaydjieva L, Giancotti F, King RH, Fejes-Toth AN, Fejes-Toth G, Feltri ML, Lang F, Salzer JL. 2014. Functionally distinct PI 3-kinase pathways regulate myelination in the peripheral nervous system. J Cell Biol 204:1219–1236. https://doi.org/10.1083/jcb.201307057.

13. Askautrud HA, Gjernes E, Gunnes G, Sletten M, Ross DT, Borresen-Dale AL, Iversen N, Tranulis MA, Frengen E. 2014. Global gene expression analysis reveals a link between NDRG1 and vesicle transport. PLoS One 9:e87268. https://doi.org/10.1371/journal.pone.0087268.

14. King RH, Chandler D, Lopaticki S, Huang D, Blake J, Muddle JR, Kilpatrick T, Nourallah M, Miyata T, Okuda T, Carter KW, Hunter M, Angelicheva D, Morahan G, Kalaydjieva L. 2011. Ndrg1 in development and maintenance of the myelin sheath. Neurobiol Dis 42:368–380. https://doi.org/10.1016/j.nbd.2011.01.030.

15. Sevinsky CJ, Khan F, Kokabee L, Darehshouri A, Maddipati KR, Conklin DS. 2018. NDRG1 regulates neutral lipid metabolism in breast cancer cells. Breast Cancer Res 20:55. https://doi.org/10.1186/s13058-018-0980-4.

16. Pietiainen V, Vassilev B, Blom T, Wang W, Nelson J, Bittman R, Back N, Zelcer N, Ikonen E. 2013. NDRG1 functions in LDL receptor trafficking by regulating endosomal recycling and degradation. J Cell Sci 126:3961–3971. https://doi.org/10.1242/jcs.128132.

17. Byun JW, An HY, Yeom SD, Lee SJ, Chung HY. 2018. NDRG1 and FOXO1 regulate endothelial cell proliferation in infantile haemangioma. Exp Dermatol 27:690–693. https://doi.org/10.1111/exd.13541.

18. Okuda T, Higashi Y, Kokame K, Tanaka C, Kondoh H, Miyata T. 2004. Ndrg1-deficient mice exhibit a progressive demyelinating disorder of peripheral nerves. Mol Cell Biol 24:3949–3956. https://doi.org/10.1128/MCB.24.9.3949-3956.2004.

19. Skedsmo FS, Espenes A, Tranulis MA, Matiasek K, Gunnes G, Bjerkas I, Moe L, Roed SS, Berendt M, Fredholm M, Rohdin C, Shelton GD, Bruheim P, Stafsnes MH, Bartosova Z, Hermansen LC, Stigen O, Jaderlund KH. 2021. Impaired NDRG1 functions in Schwann cells cause demyelinating neuropathy in a dog model of Charcot-Marie-Tooth type 4D. Neuromuscul Disord 31:56–68. https://doi.org/10.1016/j.nmd.2020.11.010.

20. Kataria H, Alizadeh A, Karimi-Abdolrezaee S. 2019. Neuregulin-1/ErbB network: an emerging modulator of nervous system injury and repair. Prog Neurobiol 180:101643. https://doi.org/10.1016/j.pneurobio.2019.101643.

21. Lee SM, Chin LS, Li L. 2017. Dysregulation of ErbB receptor trafficking and signaling in demyelinating Charcot-Marie-Tooth disease. Mol Neurobiol 54:87–100. https://doi.org/10.1007/s12035-015-9668-2.

22. Massa R, Palumbo C, Cavallaro T, Panico MB, Bei R, Terracciano C, Rizzuto N, Bernardi G, Modesti A. 2006. Overexpression of ErbB2 and ErbB3 receptors in Schwann cells of patients with Charcot-Marie-Tooth disease type 1A. Muscle Nerve 33:342–349. https://doi.org/10.1002/mus.20460.

23. Fornasari BE, Ronchi G, Pascal D, Visigalli D, Capodivento G, Nobbio L, Perroteau I, Schenone A, Geuna S, Gambarotta G. 2018. Soluble Neuregulin1 is strongly up-regulated in the rat model of Charcot-Marie-Tooth 1A disease. Exp Biol Med (Maywood) 243:370–374. https://doi.org/10.1177/1535370218754492.

24. Fledrich R, Stassart RM, Klink A, Rasch LM, Prukop T, Haag L, Czesnik D, Kungl T, Abdelaal TA, Keric N, Stadelmann C, Bruck W, Nave KA, Sereda MW. 2014. Soluble neuregulin-1 modulates disease pathogenesis in rodent models of Charcot-Marie-Tooth disease 1A. Nat Med 20:1055–1061. https://doi.org/10.1038/nm.3664.

25. Scapin C, Ferri C, Pettinato E, Zambroni D, Bianchi F, Del Carro U, Belin S, Caruso D, Mitro N, Pellegatta M, Taveggia C, Schwab MH, Nave KA, Feltri ML, Wrabetz L, D'Antonio M. 2019. Enhanced axonal neuregulin-1 type-III signaling ameliorates neurophysiology and hypomyelination in a Charcot-Marie-Tooth type 1B mouse model. Hum Mol Genet 28:992–1006. https://doi.org/10.1093/hmg/ddy411.

26. Ito H, Watari K, Shibata T, Miyamoto T, Murakami Y, Nakahara Y, Izumi H, Wakimoto H, Kuwano M, Abe T, Ono M. 2020. Bidirectional regulation between NDRG1 and GSK3beta controls tumor growth and is targeted by differentiation inducing factor-1 in glioblastoma. Cancer Res 80:234–248. https://doi.org/10.1158/0008-5472.CAN-19-0438.

27. Logan AM, Mammel AE, Robinson DC, Chin AL, Condon AF, Robinson FL. 2017. Schwann cell-specific deletion of the endosomal PI 3-kinase Vps34 leads to delayed radial sorting of axons, arrested myelination, and abnormal ErbB2-ErbB3 tyrosine kinase signaling. Glia 65:1452–1470. https://doi.org/10.1002/glia.23173.

28. Kawano S, Mizutani K, Miyata M, Ikeda W, Takai Y. 2010. Interaction of integrin alpha(6)beta(4) with ErbB3 and implication in heregulin-induced ErbB3/ErbB2-mediated DNA synthesis. Genes Cells 15:995–1001. https://doi.org/10.1111/j.1365-2443.2010.01438.x.

29. Ieguchi K, Fujita M, Ma Z, Davari P, Taniguchi Y, Sekiguchi K, Wang B, Takada YK, Takada Y. 2010. Direct binding of the EGF-like domain of neuregulin-1 to integrins ({alpha}v{beta}3 and {alpha}6{beta}4) is involved in neuregulin-1/ErbB signaling. J Biol Chem 285:31388–31398. https://doi.org/10.1074/jbc.M110.113878.

30. Guo W, Pylayeva Y, Pepe A, Yoshioka T, Muller WJ, Inghirami G, Giancotti FG. 2006. Beta 4 integrin amplifies ErbB2 signaling to promote mammary tumorigenesis. Cell 126:489–502. https://doi.org/10.1016/j.cell.2006.05.047.

31. Falcioni R, Antonini A, Nistico P, Di Stefano S, Crescenzi M, Natali PG, Sacchi A. 1997. Alpha 6 beta 4 and alpha 6 beta 1 integrins associate with ErbB-2 in human carcinoma cell lines. Exp Cell Res 236:76–85. https://doi.org/10.1006/excr.1997.3695.

32. Luigetti M, Taroni F, Milani M, Del Grande A, Romano A, Bisogni G, Conte A, Contaldo I, Mercuri E, Sabatelli M. 2014. Clinical, electrophysiological and pathological findings in a patient with Charcot-Marie-Tooth disease 4D caused by the NDRG1 Lom mutation. J Neurol Sci 345:271–273. https://doi.org/10.1016/j.jns.2014.07.042.

33. Mustonen V, Muruganandam G, Loris R, Kursula P, Ruskamo S. 2021. Crystal and solution structure of NDRG1, a membrane-binding protein linked to myelination and tumour suppression. FEBS J 288:3507–3529. https://doi.org/10.1111/febs.15660.

34. Salzer JL. 2015. Schwann cell myelination. Cold Spring Harb Perspect Biol 7:a020529. https://doi.org/10.1101/cshperspect.a020529.

35. Jones EA, Jang SW, Mager GM, Chang LW, Srinivasan R, Gokey NG, Ward RM, Nagarajan R, Svaren J. 2007. Interactions of Sox10 and Egr2 in myelin gene regulation. Neuron Glia Biol 3:377–387. https://doi.org/10.1017/S1740925X08000173.

36. Boutary S, Echaniz-Laguna A, Adams D, Loisel-Duwattez J, Schumacher M, Massaad C, Massaad-Massade L. 2021. Treating PMP22 gene duplication-related Charcot-Marie-Tooth disease: the past, the present and the future. Transl Res 227:100–111. https://doi.org/10.1016/j.trsl.2020.07.006.

37. Gouttenoire EA, Lupo V, Calpena E, Bartesaghi L, Schupfer F, Medard JJ, Maurer F, Beckmann JS, Senderek J, Palau F, Espinos C, Chrast R. 2013. Sh3tc2 deficiency affects neuregulin-1/ErbB signaling. Glia 61:1041–1051. https://doi.org/10.1002/glia.22493.

38. Kachhap SK, Faith D, Qian DZ, Shabbeer S, Galloway NL, Pili R, Denmeade SR, DeMarzo AM, Carducci MA. 2007. The N-Myc down regulated gene1 (NDRG1) is a Rab4a effector involved in vesicular recycling of E-cadherin. PLoS One 2:e844. https://doi.org/10.1371/journal.pone.0000844.

39. Gambaletta D, Marchetti A, Benedetti L, Mercurio AM, Sacchi A, Falcioni R. 2000. Cooperative signaling between alpha(6)beta(4) integrin and ErbB-2 receptor is required to promote phosphatidylinositol 3-kinase-dependent invasion. J Biol Chem 275:10604–10610. https://doi.org/10.1074/jbc.275.14.10604.

40. Bolino A, Piguet F, Alberizzi V, Pellegatta M, Rivellini C, Guerrero-Valero M, Noseda R, Brombin C, Nonis A, D'Adamo P, Taveggia C, Previtali SC. 2016. Niacin-mediated Tace activation ameliorates CMT neuropathies with focal hypermyelination. EMBO Mol Med 8:1438–1454. https://doi.org/10.15252/emmm.201606349.

41. Li HF, Chen YL, Zhuang L, Chen DF, Ke HZ, Luo WJ, Liu GL, Wu SN, Zhou WH, Xiong ZQ, Wu ZY. 2021. TMEM151A variants cause paroxysmal kinesigenic dyskinesia. Cell Discov 7:83. https://doi.org/10.1038/s41421-021-00322-w.

42. He W, Bai G, Zhou H, Wei N, White NM, Lauer J, Liu H, Shi Y, Dumitru CD, Lettieri K, Shubayev V, Jordanova A, Guergueltcheva V, Griffin PR, Burgess RW, Pfaff SL, Yang XL. 2015. CMT2D neuropathy is linked to the neomorphic binding activity of glycyl-tRNA synthetase. Nature 526:710–714. https://doi.org/10.1038/nature15510.

43. Sun SC, Ma D, Li MY, Zhang RX, Huang C, Huang HJ, Xie YZ, Wang ZJ, Liu J, Cai DC, Liu CX, Yang Q, Bao FX, Gong XL, Li JR, Hui Z, Wei XF, Zhong JM, Zhou WJ, Shang X, Zhang C, Liu XG, Tang BS, Xiong F, Xu XM. 2019. Mutations in C1orf194, encoding a calcium regulator, cause dominant Charcot-Marie-Tooth disease. Brain 142:2215–2229. https://doi.org/10.1093/brain/awz151.